Unstable periodic orbits in human epileptic activity

Michel Le Van Quyen,[1,2,*] Jacques Martinerie,[1] Claude Adam,[3] and Francisco J. Varela[1]
[1]*Laboratoire de Neurosciences Cognitives et Imagerie Cérébrale (LENA), (CNRS URA 654–University of Paris 6), Hôpital de la Salpêtrière, 47, Boulevard de l'Hôpital, 75651 Paris Cedex, France*
[2]*Hochleistungsrechenzentrum, Forschungzentrum Jülich, D-52425 Jülich, Germany*
[3]*Unité d'Epileptologie, Hôpital de la Salpêtrière, 47, Boulevard de l'Hôpital, 75651 Paris Cedex, France*
(Received 12 February 1997)

We examine in detail subdural recordings from a patient with an epileptic focal seizure, highly unusual in the ongoing nature of the discharges and in the lack of cognitive impairment. We applied a recent method for detecting unstable periodic orbits to the series of time intervals between successive spike discharges, and report that a few unstable fixed points exist within their apparent random fluctuations. The statistical significance of this underlying deterministic dynamics is assessed using surrogate data. In particular, the approaches of trajectories toward the unstable periodic patterns are observed in the sequences immediately following the perceptual tasks. This suggests that the act of perception contributes in a highly specific manner to pulling the epileptic activities towards particular unstable periodic orbits, which closely resemble the technique called chaos control for stabilization of unstable periodic orbits. [S1063-651X(97)13208-1]

PACS number(s): 87.10.+e, 05.45.+b

I. INTRODUCTION

EEG recordings are complex signals that may provide valuable information about the underlying neuronal activities. Several investigators have applied the methods coming from the field of nonlinear dynamical analysis to EEG signals recorded during different behavioral states [1]. In the case of the EEG recorded during epileptic seizures, nonlinear dynamical analysis provides a potential way to postulate some synthetic properties of the neuronal networks leading to the generation of epileptic activity [2,3]. In these studies one seeks a global measure, for example, dimension or metric entropy, of the underlying processes with the aim of distinguishing whether the EEG signal may be generated by a noise source or by a nonlinear system with deterministic dynamics. A basic limitation in these methods arises from the difficulties in characterizing local structures in the state space or rare events that are very localized in time, which are often lost when such statistical averaging methods are applied. In this work, we illustrate that detailed information about a neural dynamics can be obtained if attention is focused on exceptionally close returns of the trajectory to itself. This is motivated by the observation that chaotic systems typically have embedded within them an infinity of unstable periodic orbits [4]. In particular, a type of local geometry around an unstable periodic orbit often encountered in chaotic systems is a saddle dynamics [5] where the trajectories move toward the periodic orbit along a stable manifold and move away along an unstable manifold. Moreover, many standard techniques [6] exist to stabilize unstable periodic orbits by applying small parameter adjustments that nudge the system closer to the desired periodic state. Therefore, the ability of complex systems to access many different behaviors, combined with its sensibility, offers great flexibility in manipulating the system's dynamics to select a desired behavior [7]. In the case of complex biological systems such as the brain, the evidence of unstable orbits and the opportunity to influence their dynamics by tiny perturbations are of considerable neurobiological relevance.

Furthermore, in the context of epilepsy, if the neuroelectrical activities have a short-term predictability and this predictability can be detailed in the geometrical structure of its periodic orbits, not only does one gain an insight into the nature of the neural basis of epileptic discharges, but new therapeutic intervention can be envisaged from these dynamical patterns. In fact, it has been suggested [8] that the underlying existence of unstable periodic orbits may offer the opportunity to reduce the periodicity of a system by moving its states away from them. This basic idea (also known as ''anticontrol of chaos'') was initially tested with prior results in the hippocampal slices from a rat by direct current injections at the site of the cellular discharges [8]. Nevertheless, a more profound analysis of the epileptic dynamics is needed before definite conclusions about the underlying models may be drawn. One issue of our work is then to ask whether human epileptic activity possesses deterministic structures amenable to such anticontrol methods, which desynchronize the periodic behavior typical of epileptic seizures and perhaps suppress the seizure generation [9].

We present here a detailed study of the temporal structure of a rare case of sustained discharge from an epileptic focus recorded with subdural electrodes placed in a refractory epileptic patient. Specifically, the macroscopic electrical activities of the focus studied here display spontaneous and nearly periodic 2 Hz epileptiform discharges or spikes (Fig. 1). The generation of these focal epileptic discharges reflects sustained hypersynchronization of a localized neuronal aggregate. If this epileptic focus itself has spatial limitations, the temporal evolution of the epileptic discharges is ultimately grounded on the strong connections of these neurons with a network of neurons distributed throughout the brain. The patient under study represents then a rare occurrence to study in

*FAX: (00.49) 2461.612430. Electronic address: quyen@hlrz31.hlrz.kfa-juelich.de

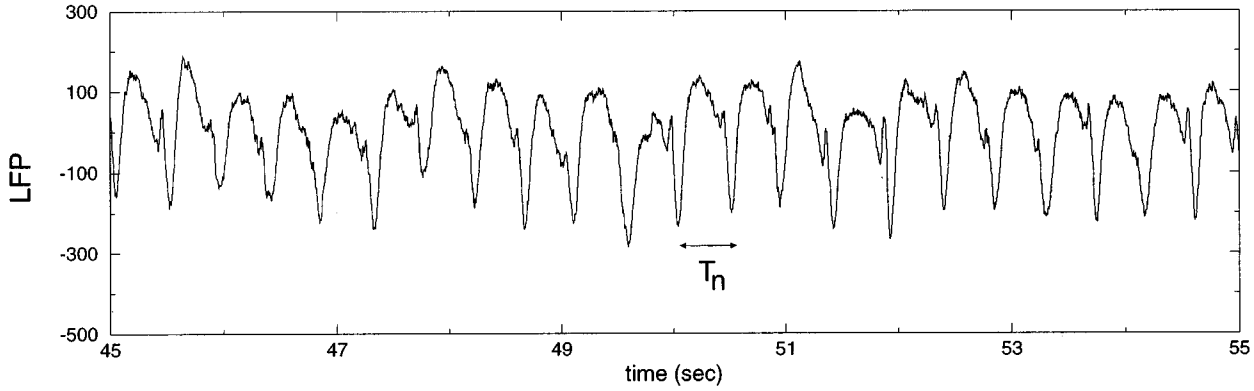

FIG. 1. 10 s of the local field recording (in μV) from the subdural electrode in the epileptogenic region. Highly stereotyped and nearly periodic epileptic discharges are continuously observed. By using the spikes as natural time markers, we studied here the time series of interspike intervals T_n.

detail the dynamics underlying the spike time series. By using the spikes as natural time markers, we can examine the small time fluctuations between these events in a time-delay plot (Sec. III). In a companion paper [10], we report significant correlations in the first return map of interspike intervals, and in particular the tendency of successive state points to cluster around a few distinct short-term periodic activities. Furthermore, the perceptual tasks the subject was requested to perform are shown to pull the epileptic activities towards specific periodicities. Our goal in the present work was designed to test whether the emergence of the periodic activities has some degree of determinism. This question is investigated here by the detection of unstable periodic orbits (Sec. IV). We test then the degree to which these patterns are related with the cognitive tasks (Sec. V).

II. EXPERIMENTAL SETUP AND CLINICAL DATA

Recordings were obtained from subdural implants of a matrix of 36 electrodes over the occipito-parietal cortex of a 23-year old male in view of surgical treatment. The signals were amplified and filtered using a 0.08–100 Hz bandpass filter, digitized at 1 kHz, and down-sampled to 3 ms. A highly stereotyped and nearly periodic epileptic discharge of spikes was continuously recorded under a single point of contact (Fig. 1) throughout the four days of preoperative monitoring without spread to adjacent contacts, suggesting a very local focus under 1 cm^2. Under axial magnetic resonance, this contact was determined to be at the junction between area 19 and the inferotemporal cortex. Respecting a protocol of informed consent, the subject was seated in a recording chamber under scotopic conditions, seated in front of a stimulation screen, and fitted with an acoustic headset. The recordings were taken in blocks comprising three consecutive experimental conditions: (A) a rest period (500 s), (B),(C) the performance of a visual and auditory discrimination task implying a finger response. For the rest condition (A) the subject was requested to remain steady while fixating on a red light on the stimulation screen. The two discrimination tasks followed an ''odd-ball'' protocol (the subject was asked to press a button as soon as he detected a rare target stimulus): For the auditory discrimination (B), a high pitch at 1 kHz target sound was briefly presented biaurally 20% of the time, randomly interleaved with a low pitch at 0.5 kHz nontarget sound presented 80% of time for a total of 400 presentations over a duration of 405 s. For visual odd-ball discrimination (C) 80 nontriangles (three ''Pacman'' shapes, presented equidistantly) were presented foveally 20% of the time (405 s), interleaved with 160 nontarget stimuli of type $N1$ (triangles drawn by lines) or 160 of type $N2$ (triangles forming a line by edge completion). As instructed, a finger response was only given when the target stimulus was presented. The patient performance for the two discrimination tasks was excellent (100% correct responses for the two discrimination tasks). For further details see [10].

III. RECONSTRUCTION OF THE DYNAMICS FROM INTERSPIKE INTERVALS

The first step toward assessing the system's dynamics is to estimate an acceptable minimum embedding dimension of the raw EEG recordings. In order to test the reliability of an embedding, one examines the number of self-crossings of the trajectories in the reconstructed state space by the method of false nearest neighbors [11]. The idea behind this test is to check whether nearest neighbors in the reconstructed state space are neighbors due to the dynamics or rather due to the projection of the original state space into a space of inappropriately low dimension. To this end, one looks for nearest neigbors in a d-dimensional space and calculates the distance of these points in a $(d+1)$-dimensional space. If the distance in the higher-dimensional space is very large, we have found a false nearest neighbor (FNN) since the two points are close in d dimensions only due to the too low-dimensional projection. The percentage of FNN over all pairs of neighbors tested should go to zero when we have found a good embedding. Using a time lag defined by reconstruction expansion [12], we use all data sets to discover the percentage of FNN shown in Fig. 2. For the three EEG signals, there is a sharp drop to zero at dimension 4 after which the percentage of FNN remains zero. This provides evidence that a low embedding dimension is able to capture the features of the data observed.

The decomposition of a given signal into several characteristic events may bring valuable information [13]. In the epileptic activities, peaks of the activity, or spikes, and interspike periods are distinguable events with considerable neu-

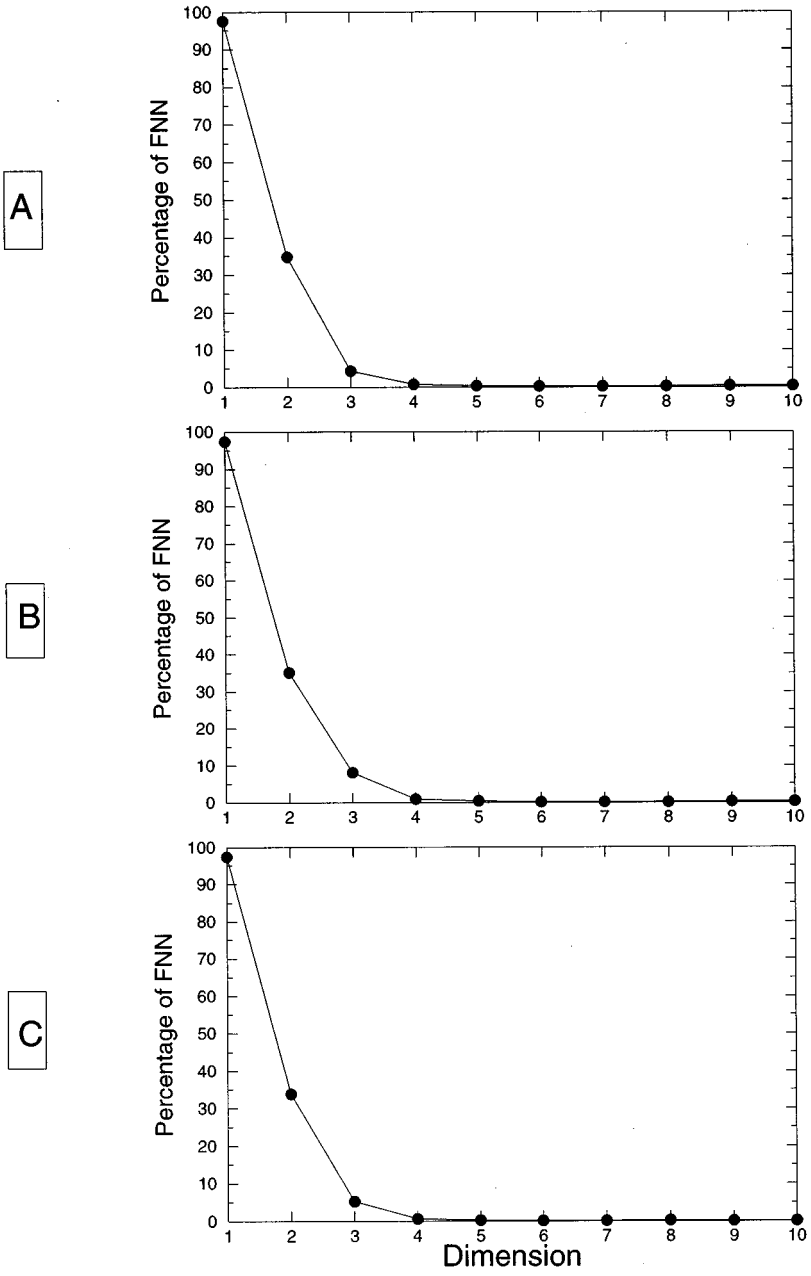

FIG. 2. Percentage of false nearest neighbors (FNN) as a function of embedding dimension for the EEG recordings in the resting (A), auditory (B), and visual (C) discrimination conditions. For the three EEG signals, there is a sharp drop to zero at dimension 4 after which the percentage of FNN remains zero. For the computation, we used the threshold sizes $R_{\mathrm{tol}}=10$ and $A_{\mathrm{tol}}=2$ (see Ref. [11] for details). The time lag is defined here by the method of reconstruction expansion [12].

robiological and clinical significance. The succession in time of these events is very important for understanding the separate underlying physiological processes. In the study here, the ongoing and localized spikes produced by the epileptic focus provide an opportunity to study the dynamics of succession of interspike intervals. To obtain the intervals between spikes T_n from the continuous outputs (Fig. 1), we follow Sauer [14] and pass the voltages through a threshold detector, which outputs a narrow pulse each time a positive-going threshold crossing occurs. We studied then the time series of interspike intervals $\{T_n\}_{n=1}^{N}$ [conditions (A) $N=1062$, (B) $N=887$, (C) $N=851$]. These time series exhibit a considerable cycle-to-cycle variability around a mean, as clearly seen when plotted in a cumulative histogram [Fig. 3(a)]. There are no significant differences in the mean [conditions (A) $m=0.470$ s, (B) $m=0.475$ s, (C) $m=0.456$ s] and dispersion values [conditions (A) $\sigma=0.038$ s, (B) $\sigma=0.047$ s, (C) $\sigma=0.056$ s] among the three study conditions.

From the perspective of nonlinear dynamics, that delay embedding of the interevent intervals may also be used to reconstruct the dynamics of a system was recently demonstrated [14]. When a chaotic signal is fed into a threshold crossing detector, the time-delay plot of time intervals between crossings reconstructs a Poincaré section of the underlying dynamics. We consider here a first return map of two successive intervals, T_{n+1} versus T_n [Fig. 3(b)], and then the sequence of state points (T_n, T_{n+1}) displayed in this map can be interpreted as a projection of the original low-dimensional state-space trajectory. We do not expect here to fully disentangle all trajectories of the dynamics with a two-dimensional embedding, but, as in other previous work [8,15,16], we are ultimately interested in the geometric properties of low-period orbits, which could be identified in the first-return map.

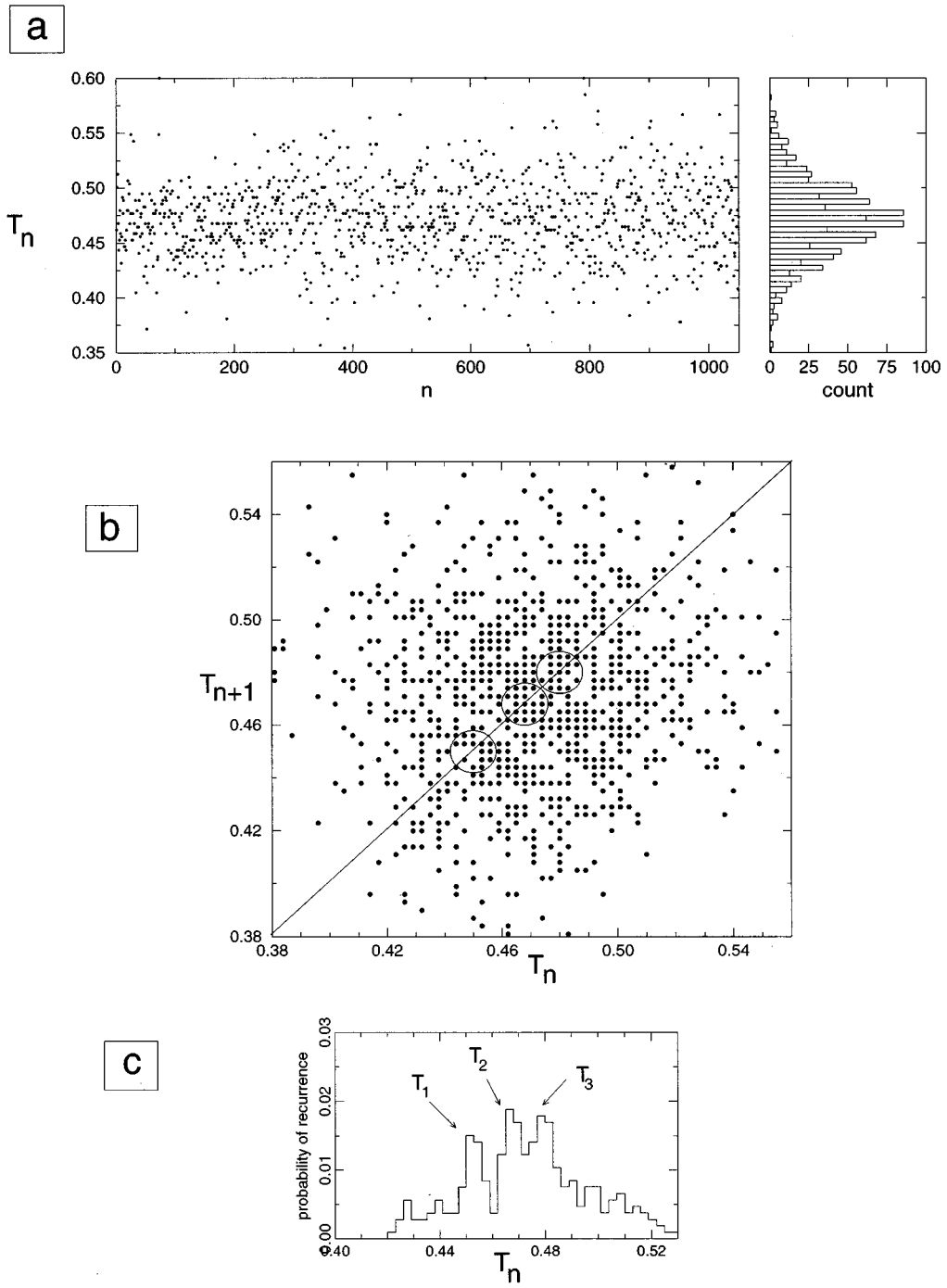

FIG. 3. (a) The full data sets of interspike intervals $\{T_n\}_{n=1}^{N}$ ($N=1062$ spikes) and the interspike interval histogram for the resting condition (A). Notice that T_n exhibit a considerable cycle-to-cycle variability around the mean $m=0.47$ s. (b) First return map T_{n+1} vs the previous T_n for the resting condition. (c) Density of points in the return map located within a small circle (of radius 8 ms) around a particular value T of the diagonal. This density indicates the probability that successive intervals will remain around a chosen time T. Three main probability peaks T_1, T_2, T_3 are marked with arrows and indicated with circles in the return map. The inhomogeneous clustering of the points is a significant indication that successive interspike intervals are correlated.

IV. DETECTING UNSTABLE PERIODIC ORBITS

In the first return map, the diagonal line is the locus where two intervals are identical $T_n=T_{n+1}$; an accumulation of points are traces of 1-periodic activity. In contrast, if the density is uniform along vertical lines, the probability of interval T_{n+1} is independent of the value of the previous interval T_n, and there is no trace of correlated activity. A visual examination of the first return plots for the various conditions shows accumulations of points into a few distinct groups that cluster around discrete positions along the diagonal [Fig. 3(b)]. More precisely, we estimate the density of points in the return map located within a small circle (radius of 8 ms) around a particular value T of the diagonal. This density tells us the probability that pairs of successive intervals will remain around a chosen value T. As shown in Fig. 3(c) not all values of T have similar probabilities, thus sig-

nifying that successive spikes are correlated since recurrence times fall into three evenly spaced distinct peaks T_1, T_2, T_3 (corresponding, respectively, to periodicities around 0.45, 0.465, and 0.48 s). These three peaks can be also found in all experimental conditions, and are most clearly seen during the auditive and visual discrimination tasks [10]. These recurrence times may reflect the presence of unstable fixed points. Nevertheless, sequences that resemble fixed points can also be observed in stochastic correlated data [17]. In order to establish whether the fixed point sequences observed in the data arise from occasional chance correlations between successive data points, we further consider the trajectories in the neighborhood of the recurrence points, and also examine the statistical significance of the detections in order to avoid subjective selection. A simple method for detecting unstable orbits was recently introduced by So *et al.* [18]. This method utilizes a transformation of the experimental time series T_n:

$$\overline{T_n} = [T_{n+1} - s_n(k) T_n]/[1 - s_n(k)], \tag{1}$$

where

$$s_n(k) = (T_{n+2} - T_{n+1})/(T_{n+1} - T_n) + k(T_{n+1} - T_n). \tag{2}$$

All points that lie in the linear region of a fixed point T^* will be transformed to the vicinity near T^*. Thus if we plot a histogram $\rho(\overline{T_n})$ of the transformed time series $\overline{T_n}$ there will be a sharp peak at $\overline{T} = T^*$. Thus in contrast to typical ''recurrence'' based methods [4,5], the transformation in Eqs. (1) and (2) utilizes by construction all the points in the linear region of a fixed point to form a peak. Since spurious peaks depend on the parameter k but not on the true peak at the fixed point, the spurious peaks will be eliminated to randomly pick many different $k = \kappa R$ with R chosen randomly in $[-1,1]$ for each $\overline{T}$ value, and form the average over k, $\langle \rho(\overline{T}) \rangle_k$, of the resulting distributions. The reliability of this detection of fixed points can be further assessed by testing the statistical significance of the peaks against carefully constructed controls. We want particularly to exclude detection in our data that can be accounted for linear correlation in time. Thus, we have used the method of surrogate data [19] for the generation of two types of control signals where linear properties of the data are preserved (i.e., autocorrelation, power spectrum), yet the data are randomized to destroy deterministic structure that may be present. In the first type (type I of Ref. [19]), a random phase is added to each complex coefficient of the Fourier transform and an inverse Fourier transform then generates a new random time series. The second type of surrogate (type II of Ref. [19]) assumes that the data came from a normally distributed random process that was filtered through a nonlinear filter. If our methods cannot distinguish surrogate series from the observed series, then the result provides no evidence for underlying deterministic unstable periodic orbits. We denote by $\langle \rho_{\mathrm{orig}}(T) \rangle$ the statistic calculated for each point T of the original time series, and $\langle \rho_{\mathrm{sur}}(T) \rangle$ for the surrogates; the significance can then be estimated by a one-tailed Monte Carlo test [20]:

$$P = \frac{(\text{number of case}\{\langle \rho_{\mathrm{sur}}(T) \rangle \geqslant \langle \rho_{\mathrm{orig}}(T) \rangle\}) + 1}{(\text{number of surrogate}) + 1}. \tag{3}$$

Here 39 different realizations of each type of surrogate data set are produced. If $\langle \rho_{\mathrm{orig}}(T) \rangle$ is greater than all surrogate results for a particular value of T, then we can reject at a significant level of $P = 0.025$ the null hypothesis that the detection of periodic orbits in the data can be explained by a simple linear stochastic process modeled by the surrogates, and assume deterministic structures to be present. The results of the detection of fixed points are shown in Fig. 4 for the three experimental conditions (A)–(C). The lower plots show the histograms $\langle \rho(\overline{T}) \rangle$ of the transformed time series as a solid curve, and the surrogates' mean histograms are plotted as dotted and dashed curves. The upper plots in each condition show the degree of statistical confidence of the detection [defined as $100(1-P)\%$ in the figure]. Arrows indicate the values where the detection is positively confirmed by the rejection (at a level of 97.5%) of the two null hypotheses defined by the surrogates. During the resting condition (A), three distinct peaks at T_1, T_2, and T_3 [corresponding to the related recurrence times observed Fig. 3(c)] are discernible, but only the peak located at $T_3 = 0.48$ s was deemed to be statistically significant for an unstable fixed point. During the visual discrimination tasks (C), the same three time intervals have strong peaks rising sharply above the surrogates' means where the significance of unstable fixed points is clearly demonstrated. During the auditive discrimination tasks (B), only a sharp peak at $T_2 = 0.46$ s gives a positive result for the significance of fixed points.

The principal aspect of the significance of these dynamical patterns can be directly obtained by examining individual short sequences of points around the diagonal. A typical example of recurrent observed trajectories is shown for point T_2 in Fig. 5, displaying the sequence of points numbered 717–721. From points 717–719, the state of the system is drawn toward the diagonal along a specific linear slope, but after point 719 it diverges away from the diagonal with a different slope. Other sequences of points moving toward the fixed points T_2 and T_3 along a line and outward along another line are shown in Fig. 5. This direct observations revealed that the trajectories around the fixed points look very much like motion near a fixed point of the saddle focus type with stable and unstable manifolds that intersect at the fixed point. More precisely, the bottom of Fig. 5 shows the cumulative histograms of the steepness of the approach and departure related to the two points T_2 and T_3. These slopes were calculated by least-squares line fits of three sequential points with the condition that the intersection with the diagonal must lie within a circle of specified radius (here 8 ms) centered at the location of the fixed point. We can see that the steepness of the approach has in each time series a prominent peak. Further, these peaks were markedly similar across the different series in the resting (A), auditive tasks (B), and visual tasks (C) for each fixed point examined. Similar results were obtained for the steepness of departure, but the short sequences of divergence make it more difficult to accurately estimate their slope. In a two-dimensional plot, the slopes of approach and departure are numerically equal to the eigenvalues at the fixed point. For the all-fixed-point se-

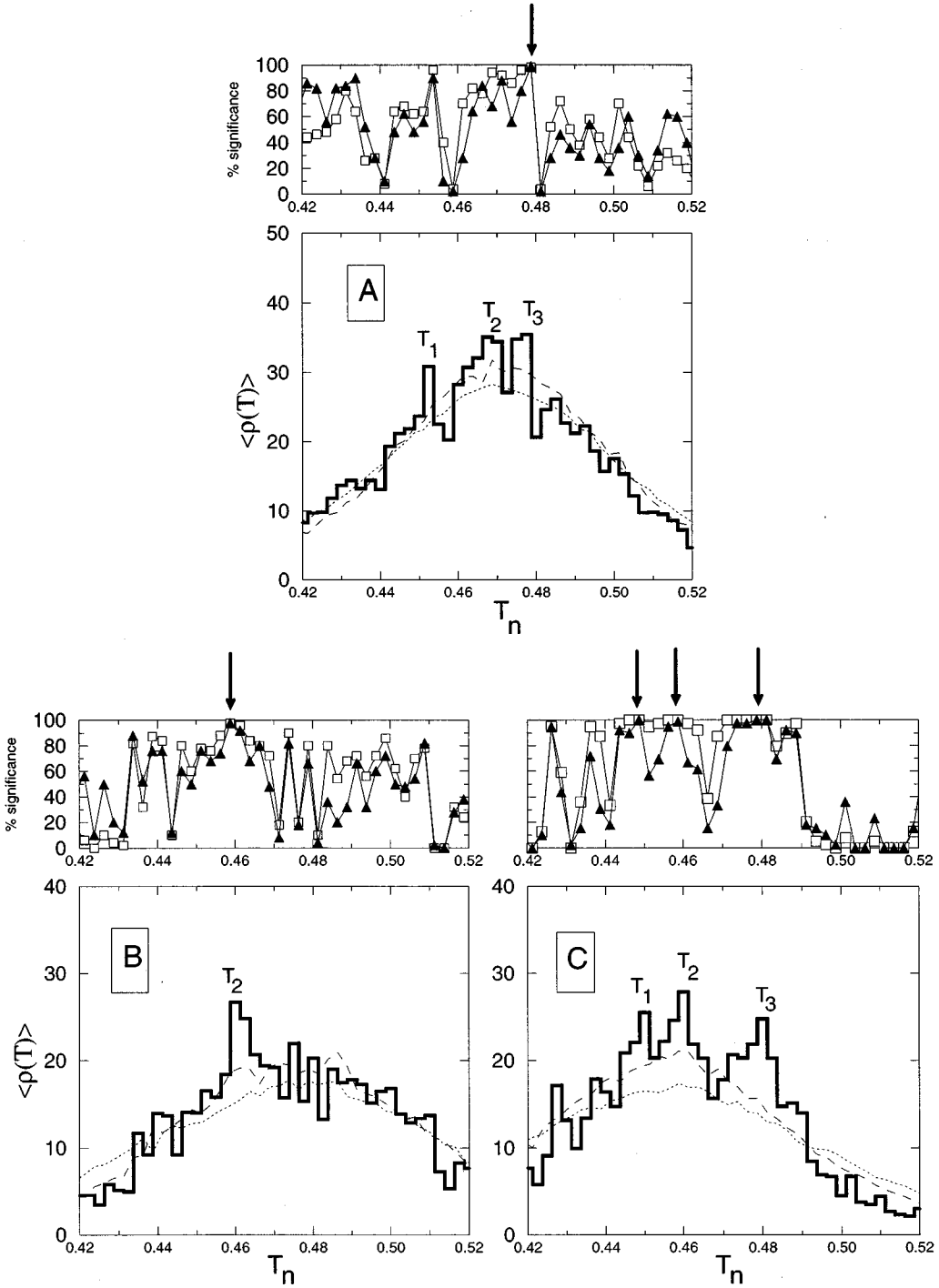

FIG. 4. Histogram plots of the transformed time series $\langle \rho(\overline{T}) \rangle_k$ (arbitrary units) averaged over 500 values of k, where $k=5R$, $R \in [-1,1]$, for the resting (A), auditory (B), and visual (C) discrimination conditions. For each time series, we applied the detection method of periodic orbits to the original data and to two groups of 39 truly stochastic data (surrogates of type I and type II) with similar statistical properties. The lower plots show the histograms of the transformed time series as a solid curve, and the surrogates' mean histograms are plotted as dotted curves (type I) and dashed curves (type II). The upper panels determine the significance of unstable fixed point against each null hypotheses (squares, surrogate of type I; black triangles, surrogates of type II). Arrows indicate the values where the null-hypothesis (at a confidence level of 97.5%) can be rejected for the two types of surrogates.

quences in the three time series, we estimated the following stable eigenvalues: for T_1, $\lambda_s = -0.41 \pm 0.18$; for T_2, $\lambda_s = -0.45 \pm 0.12$; for T_3, $\lambda_s = -0.47 \pm 0.11$. We estimated the following unstable eigenvalues: for T_1, $\lambda_u = -3.03 \pm 0.56$; for T_2, $\lambda_u = -3.11 \pm 0.74$; for T_3, $\lambda_u = -3.08 \pm 0.55$.

V. EFFECT OF SPECIFIC STIMULUS CONDITIONS

The epileptic focus is reciprocally connected to other more or less distant neural sources and is part of an extended network of neural activities that exert their modulation. As reported in a companion paper [10], the small-scale changes

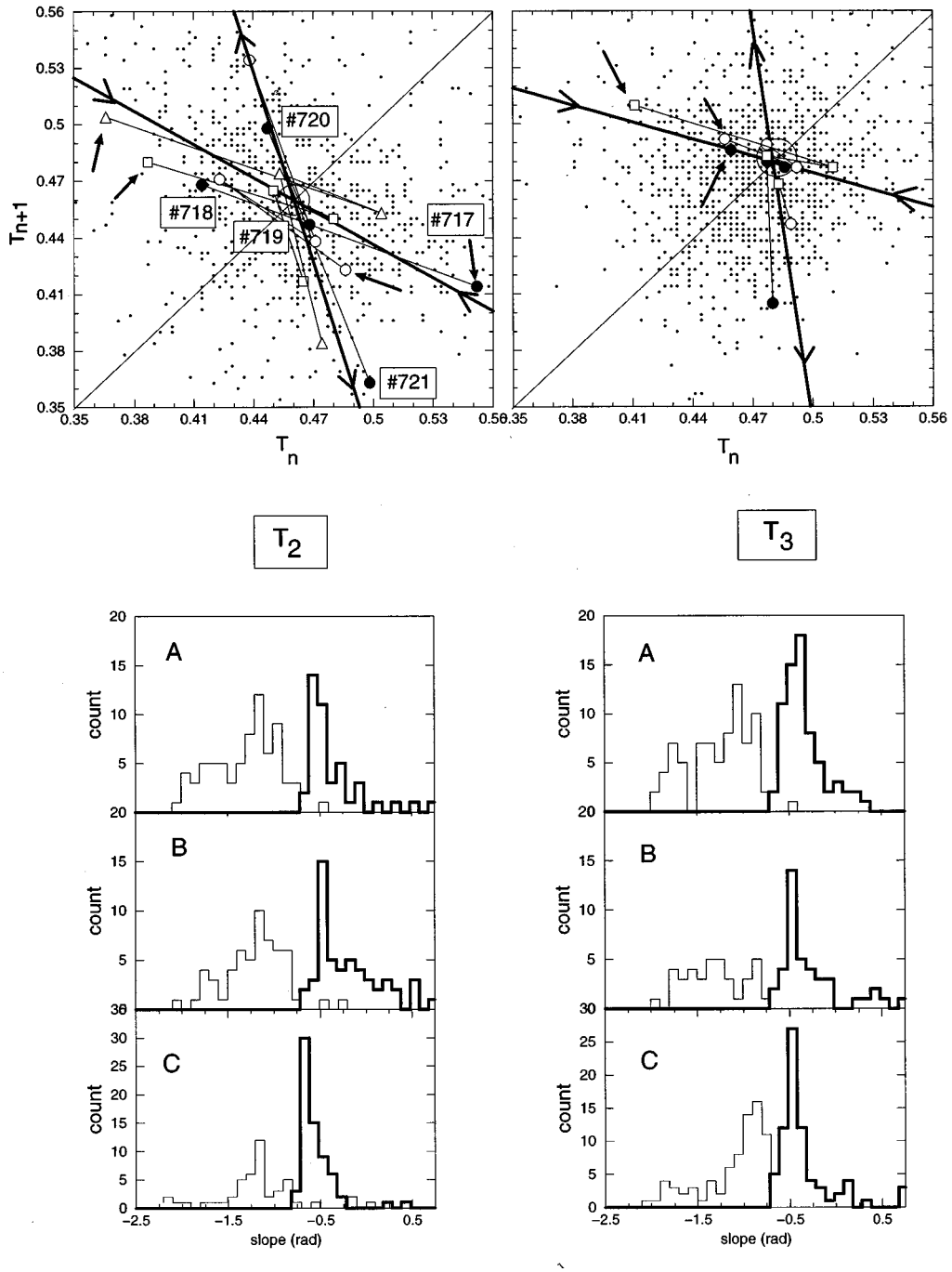

FIG. 5. Top: first-return map showing visitations of two particular fixed points, $T_2 = 0.465$ s and $T_3 = 0.48$ s. For each sequence, the starting points are indicated by arrows. Multiple trajectories (here symbol coded) that did not follow each other in time approach the neighborhood along a stable direction and diverge away along a different unstable direction (see, for instance, T_2, points 717–720, black circles). The stable and unstable manifolds are estimated by straight line fits to all the visitations, and are indicated by a heavy black line with arrows pointing toward the unstable fixed points or by arrows pointing away from the fixed point. Bottom: histograms of the slopes of approach (heavy) and departure (light) of T_2 and T_3 calculated with straight line fits to sequences of 3 points moving toward or moving away from a small circle (radius 8 ms) around the fixed points. We can see that the steepnesses of the visitation direction have in each time series two prominent peaks. Further, these peaks were markedly similar across the different series (A), (B), and (C).

in the internal structure of the epileptic spike pattern reflect the cognitive tasks. Accordingly, the previous section shows also clear changes in the significance of the unstable fixed points [for example, between conditions (B) and (C)]. In this section, we examine in the return map the segments of the trajectories directly related with the discrimination tasks. The first step toward assessing task-related events in the interspike intervals is to separately analyze the target and non-target presentations for effects of condition. To do this, we consider the interspike intervals T_i corresponding to the target (nontarget) presentation number i (80 target and 320 nontarget stimulations for a total of 400 presentations) and observe in the intervals immediately following $\{T_{i+k}\}_{k=0,\ldots,p-1}$ the presence of an unstable fixed point by

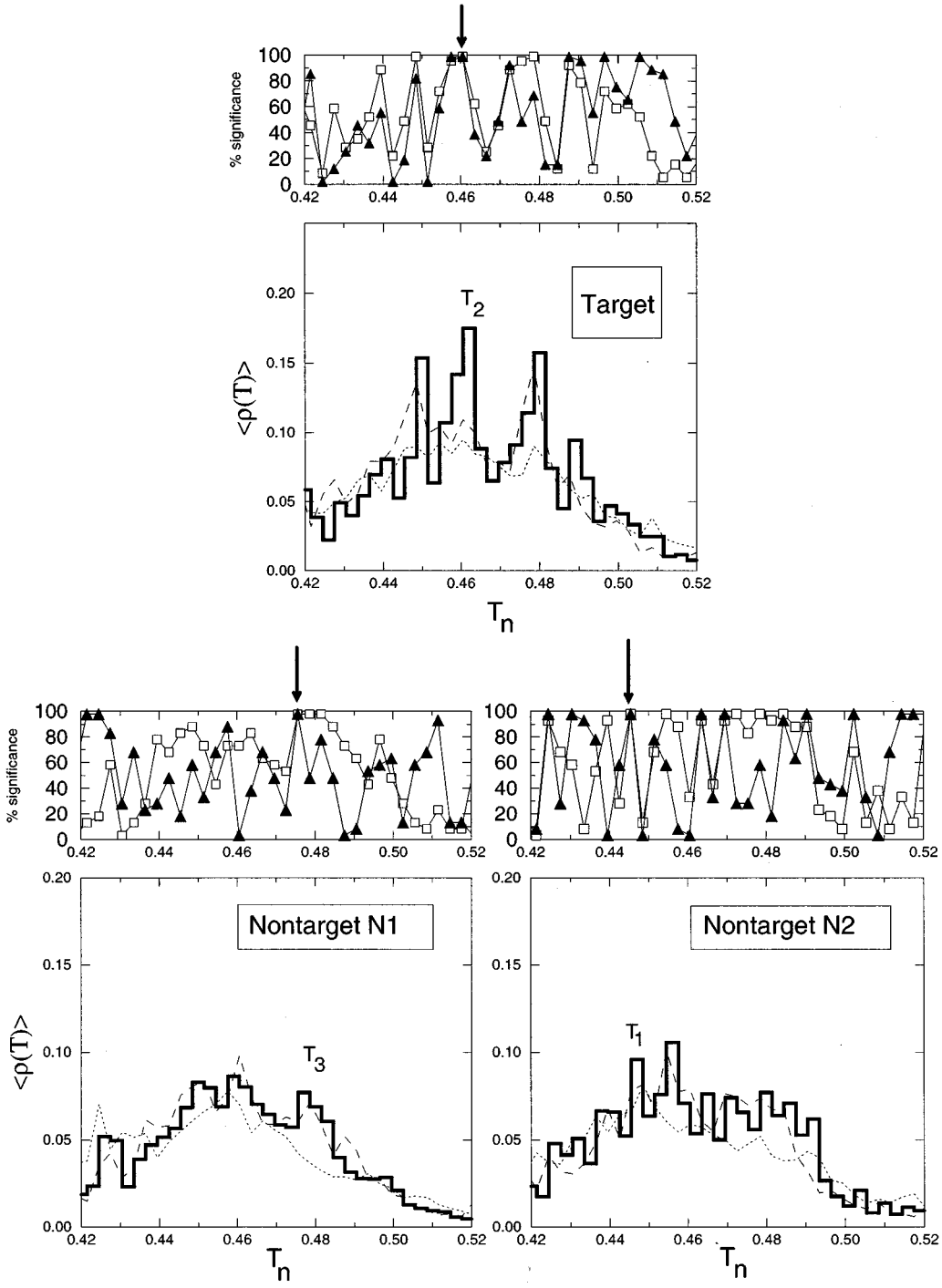

FIG. 6. Histogram plots $\langle \rho(\overline{T}) \rangle_k$ (solid curve) averaged over 500 values of k, $k=5R$, $R \in [-1,1]$, for interspike intervals directly following the visual target, nontarget of type $N1$, and nontarget of type $N2$ presentations. Two types of surrogate are used: The type a surrogates were obtained by scrambling the order of intervals in the sequences following a task. The type b are obtained by randomly choosing the times of target or nontarget presentations. The mean histogram of 39 surrogates is plotted as dotted curves for type a and dashed curves for type b. The upper panels show the significance of unstable fixed point against the null hypothesis (squares, surrogate of type a; black triangles, surrogates of type b). Arrows indicate the values where the null hypothesis (at confidence level of 97.5%) can be rejected for the two types of surrogates.

the same method as in the previous section. We set here $p=4$. Because the time series considered are extremely short, the surrogate algorithms previously used are not reliably applicable. Here statistical controls were obtained by scrambling the order of intervals in the sequences following a task (type a). The null hypothesis is then that there is no dynamical correlation at all from one interval to another. A second form of surrogate data to investigate significant effects following a stimulus presentation is further obtained by randomly choosing artificial times of target or nontarget presentations (type b). The null hypothesis is that there is no correlation between the timings of stimulus presentation and

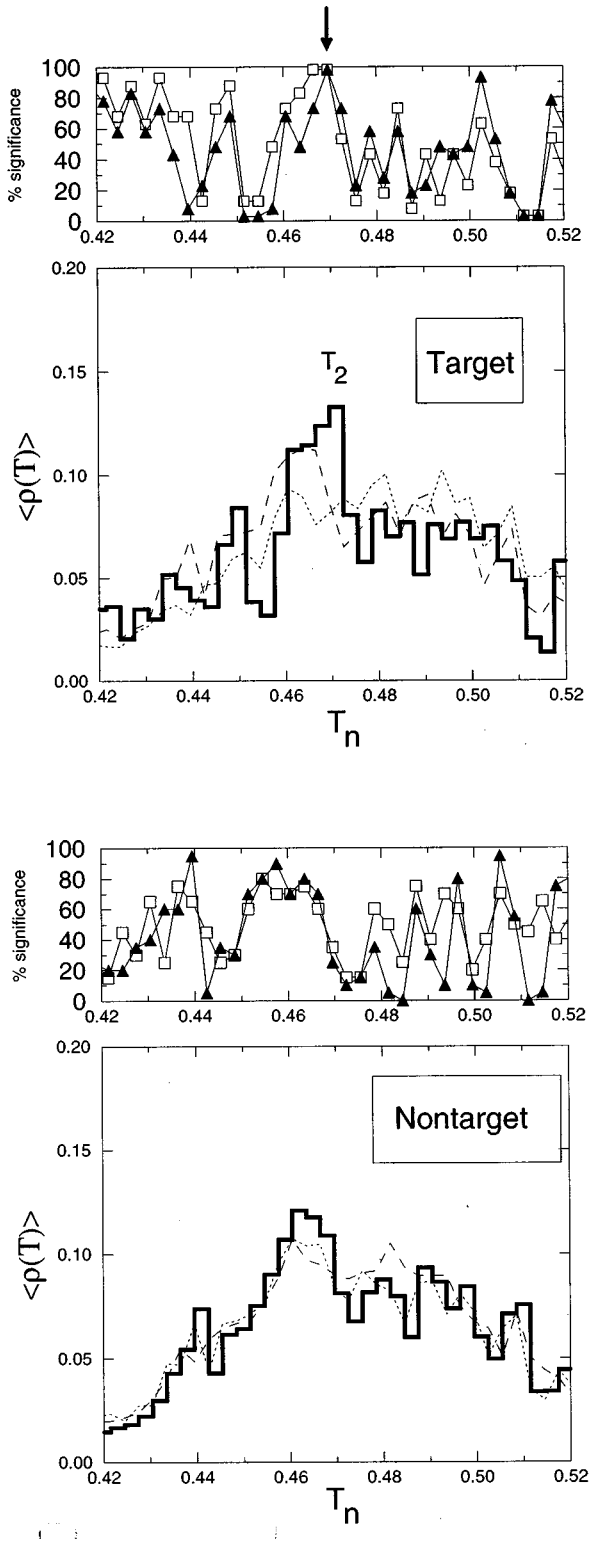

FIG. 7. Histogram plots $\langle \rho(\overline{T}) \rangle_k$ for interspike intervals directly following the auditive target and nontarget presentations, the same parameter values and legends as in Fig. 6.

the related interspike intervals. The results of the detection of fixed points are shown in Fig. 6 for the visual tasks, and Fig. 7 for the auditive tasks. The plots show the cumulative histograms (normalized over the number of stimulations) of all the transformed time series for target and nontarget stimulations, and also the degree of statistical confidence that the original data can be distinguished from the statistical controls.

As shown in Fig. 6, when this analysis was applied to the visual target presentations using the type *a* surrogates, the existence of statistically significant unstable fixed points was particularly pronounced for the three peaks at T_1, T_2, and T_3. However, the type *b* surrogate test shows that only one peak at T_2 is directly associated with the visual target presentations. In the case of the visual nontarget presentations of type $N1$, one significant peak at T_3 was common to both surrogate tests. In the case of the nontarget presentations of type $N2$, a significant effect was also demonstrated for one peak at T_1. Shown in Fig. 7, similar computations were performed for the auditive stimulations. The trajectories associated with target presentations exhibit one significant peak near T_2 for both surrogates. In contrast, peaks were virtually absent for the nontarget presentations. In sum, these results reveal a striking one-to-one association between a given sensory stimulus presentation and a specific unstable periodic orbit. It follows that in this patient a particular visual or auditive stimulus acted to drive the epileptic activity into various patterns of specific short-time periodic activity.

VI. DISCUSSION

A. Dynamical patterns and epileptic mechanisms

The timing of discharges of the focal epilepsy analyzed here has provided consistent indications that the dynamics underlying spike generation is not a simple noise-perturbated limit cycle, but contains episodes of deterministic dynamics. The identification of specific events that cannot be detected with traditional linear models provides a synthetic characterization of the discharges generated by neuronal populations in the site of focus, as well as long-range modulation from other connections in the brain. In spite of the fact that the simplicity of the first-return map used here cannot fully disentangle all trajectories of state space, it does reveal local regions where it may be possible to make predictions a few cycles away. The validity of the first return plot is further supported by the evidence of the low dimensionality of the raw EEG recordings. Return maps of time intervals between the occurrences of pulses are also explored by other recent works [8,16,21]. Furthermore, nonlinear predictions of future values have already been shown for neuronal discharges in the study of spinal cord reflexes and hippocampal slices [22]. In addition, our results address the idea that the local temporal dynamics underlying the epileptic spikes are characterized by a tendency to fall into trajectories that approach a few periodic points along a specific slope, and remain nearby for a brief time before they diverge away. Although the significance of the periodic points differs slightly among the behavioral conditions studied, these local structures appear as invariant features of the dynamics for all our experimental conditions, and thus reflect a consistent physiological basis. This picture from human subdural recordings during awake behavior is quite comparable to the detection of an unstable fixed point described in rats' brain slices [8,15]. We also assess the reliability of the detection of deterministic events by testing these statistical significances against surrogate data that are random but preserve statistical properties of the original data.

B. Unstable periodic orbits evoked by perceptual tasks

A particularity of the present work is that the EEG recordings of spike generation have been obtained under controlled circumstances during cognitive responses. A result of our study is that subtle changes in the dynamics of the epileptic interspike intervals are associated with stimulus presentations. Consistent with our analysis of the periodic clusters in successive discharge intervals [10], our case study shows here that a given sensory stimulus contributes to triggering the trajectories in the state space towards specific unstable periodicities. In our epileptic patient, only one unstable periodic orbit is detected during the rest condition. In contrast, during the visual discrimination task, 3–4 periodic orbits with their local deterministic structures emerge. Since the focal discharges were located in the visuotemporal region, it was to be expected that effects can be detected during the visual discrimination tasks. These increases in the dynamical complexity of the neuronal dynamics in relation to mental activity are in agreement with other recent studies [23]. Furthermore, our findings of the dependence of dynamics on stimulus add support to the conjecture [24] that epileptic activities are partially under the control of the brain's ongoing activity and suggest that the generation of a specific temporal pattern in the epileptic discharges could be related to cognitive activity. This hypothesis is also indirectly supported by clinical obervations of seizures following auditory and visual stimulations, mental operation, or self-induced suggestions [25]. In these cases, our work suggests that a particular cognitive task may drive the neuronal activities to specific periodic behaviors, which can culminate in a pattern of synchronous activation of a more extensive population of neurons. From a more general point of view, other transitions of brain activities into occasional coherent oscillatory states and induced by sensory stimulus can be also interpreted as approaches of the neuronal dynamics toward low unstable periodic orbits [26]. An example along this direction is provided by the work of Freeman on the large-scale collective behavior of the rabbit's olfactory system [27]. Most of the time, the EEGs at the surface of the olfactory bulb showed irregular spatiotemporal activities. However, when the animal inhaled a familiar odor, the electrical activities in each EEG recording became more regular for a brief period until the animal exhaled. In fact, the ability of the brain to access many different unstable states and to alternate among them offers a great flexibility in the control and selection of a desired behavior. Interestingly, these observations can be understood in the theoretical perspective of controlling chaos, which exactly uses the unstable periodic orbits to convert an irregular dynamics of a system to a time-periodic one. Indeed, models of neuronal networks show that different synchronized oscillations could be switched on and off rapidly under the action of small perturbations by the techniques of chaos control [28].

C. Therapeutic interventions

Several authors have advanced the view that, for some physiological systems, a highly complex behavior is related to normality, while transitions to a lower complexity such as a nearly periodic behavior are viewed as a pathological loss of the range of adaptive possibilities (or ''dynamical diseases'' [29]). From this perspective, the epileptic seizure with its massive rhythmic depolarization may be considered as the expression of pathological corrective mechanisms. Motivated by this, recent studies [30,31] investigate the possibility of using small control perturbation to preserve chaotic motion or to redirect the system to a condition of higher complexity. Known as ''anticontrol of chaos,'' these techniques have successfully exploited specific locations in the state space for the maintenance of complexity in physical systems. The method is based on perturbing a trajectory to an attractive periodic point with a small change in some system parameter so that it will fall away from its neighborhood, and then offer the ability to break up periodic behavior. More to the point, delivering low-amplitude regularly timed electrical stimulations, Schiff [8] *et al.* were able to anticontrol the seizurelike neuronal discharges in slices of rat hippocampal tissue, by perturbing a stable orbit, so that the next state point falls close to the unstable direction, with a corresponding transition from periodic to complex behavior. Because the epileptic focus studied here displays comparable unstable periodic orbits, we believe that similar strategies may eventually be applied to such foci. In a clinical environment with a small array of electrodes already implanted in the patient, anticontrol techniques to maintain the trajectories of the epileptogenic focus away from short-term periodic activities are open as a realistic strategy [9] eventually combined with modulation from selected cognitive tasks capable of reliably inducing trajectory changes. Our future work will further explore these pertinent issues.

[1] L. Glass, in *The Handbook of Brain Theory and Neural Networks*, edited by M. A. Arbib (MIT Press, Cambridge, MA, 1995), pp. 186–189.
[2] F. Lopes da Silva and J. P. Pijn, in *The Handbook of Brain Theory and Neural Networks* (Ref. [1]), pp. 367–369.
[3] G. W. Frank, T. Lookman, M. Nerenberg, C. Essex, J. Lemieux, and W. Blume, Physica D **46**, 427 (1990); J. P. Pijn, J. V. Neerven, A. Noest, and F. H. Lopes da Silva, Electroencephalogr. Clin. Neurophysiol. **79**, 371 (1991).
[4] D. Auerbach, P. Cvitanovic, J. P. Eckmann, G. Gunaratne, and I. Procaccia, Phys. Rev. Lett. **58**, 2387 (1987).
[5] D. P. Lathrop and E. J. Kostelich, Phys. Rev. A **40**, 4028 (1989).
[6] E. Ott, C. Grebogi, and J. Yorke, Phys. Rev. Lett. **64**, 1196 (1990); A. Garfinkel, M. L. Spano, W. L. Ditto, and J. Weiss, Science **257**, 1230 (1992).
[7] L. Poon and C. Grebogi, Phys. Rev. Lett. **75**, 4023 (1995).
[8] S. J. Schiff, K. Jerger, D. H. Duong, T. Chang, M. L. Spano, and W. L. Ditto, Nature (London) **370**, 615 (1994).
[9] J. Glanz, Science **265**, 1174 (1994).

[10] M. Le Van Quyen, C. Adam, J. P. Lachaux, J. Martinerie, M. Baulac, B. Renauld, and F. Varela, Neuroreport **8**, 1703 (1997).
[11] M. B. Kennel, R. Brown, and H. D. Abarbanel, Phys. Rev. A **45**, 3403 (1992).
[12] M. T. Rosenstein, J. J. Collins, and C. J. De Luca, Physica D **73**, 82 (1994).
[13] R. S. Shaw, *The Dripping Faucet as a Model Dynamical System* (Aerial Press, Santa Cruz, CA, 1984).
[14] T. Sauer, Phys. Rev. Lett. **72**, 3811 (1994).
[15] H. Hayashi and S. Ishizuka, Brain Res. **686**, 194 (1995); S. Ishizuka and H. Hayashi, *ibid.* **723**, 46 (1996).
[16] D. Pierson and F. Moss, Phys. Rev. Lett. **75**, 2124 (1995).
[17] D. J. Christini and J. J. Collins, Phys. Rev. Lett. **75**, 2782 (1995).
[18] P. So, E. Ott, S. J. Schiff, D. T. Kaplan, T. Sauer, and C. Grebogi, Phys. Rev. Lett. **76**, 4705 (1996).
[19] J. Theiler, S. Eubank, A. Longtin, B. Galdrikian, and J. D. Farmer, Physica D **58**, 77 (1992).
[20] A. Hope, J. R. Statistical Soc. B **30**, 582 (1968).
[21] F. X. Witkowski, K. M. Kavanagh, P. A. Penkoske, R. Plongey, M. L. Spano, W. Ditto, and D. T. Kaplan, Phys. Rev. Lett. **75**, 1230 (1995).
[22] T. Chang, S. J. Schiff, T. Sauer, J. P. Gossard, and R. E. Burke, Biophys. J. **67**, 671 (1994).
[23] C. J. Stam, T. C. van Woerkom, and W. S. Prichard, Electroencephalogr. Clin. Neurophysiol. **99**, 214 (1996).
[24] C. D. Binnie and D. Marston, Epilepsia Suppl. **33**, 11 (1993).
[25] A. Beaumanoir, H. Gastaut, and R. Naquet, *Reflex Seizures and Reflex Epilepsies* (Editions Médicine et Hygiène, Genève, 1989).
[26] F. J. Varela, Biol. Res. **28**, 81 (1995).
[27] W. J. Freeman, Electroencephalogr. Clin. Neurophysiol. **44**, 586 (1980).
[28] C. Lourenço and A. Babloyantz, Neural Comput. **6**, 1141 (1994).
[29] M. Mackey and L. Glass, Science **197**, 287 (1977).
[30] W. Yang, M. Ding, A. J. Mandell, and E. Ott, Phys. Rev. E **51**, 102 (1995).
[31] V. In, S. E. Mahan, W. L. Ditto, and M. L. Spano, Phys. Rev. Lett. **74**, 4420 (1995).